Self-Assembly of Nanoparticle Amphiphiles with Adaptive Surface Chemistry

Hee-Young Lee,[†] Sun Hae Ra Shin,[†] Aaron M. Drews, Aaron M. Chirsan, Sean A. Lewis, and Kyle J. M. Bishop*

Department of Chemical Engineering, The Pennsylvania State University, University Park, Pennsylvania 16802, United States. [†]These authors contributed equally.

ABSTRACT We investigate the self-assembly of amphiphilic nanoparticles (NPs) functionalized with mixed monolayers of hydrophobic and hydrophilic ligands in water. Unlike typical amphiphilic particles with "fixed" surface chemistries, the ligands used here are not bound irreversibly but can rearrange dynamically on the particles' surface during their assembly from solution. Depending on the assembly conditions, these adaptive amphiphiles form compact micellar clusters or extended chain-like assemblies in aqueous solution. By controlling the amount of hydrophobic ligands on the particles' surface, the average number of nearest neighbors—that is, the preferred coordination number—can be varied systematically from ~1 (dimers) to ~2 (linear chains) to ~3 (extended clusters). To explain these experimental findings, we present an assembly mechanism in which hydrophobic ligands organize dynamically to form discrete patches between proximal NPs to minimize contact with their aqueous surroundings. Monte Carlo simulations incorporating these adaptive hydrophobic interactions reproduce the three-dimensional assemblies observed in experiment. These results suggest a general strategy based on reconfigurable "sticky" patches that may allow for tunable control over particle coordination number within self-assembled structures.

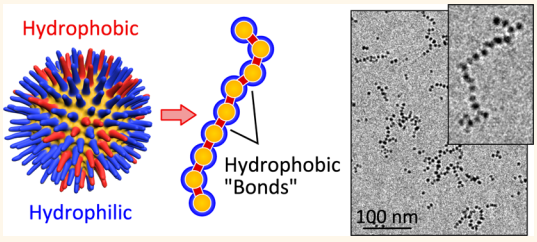

KEYWORDS: patchy particles · Janus particles · mixed monolayers · hydrophobic interactions · surfactants

Amphiphilic particles self-assemble to form a variety of structures—clusters,[1−3] helices,[2] vesicles,[4−6] and open lattices[7]—depending on their shape[8,9] and on the distribution of hydrophilic and hydrophobic regions decorating their surface. Typically, the hydrophobic "patches" on the particles' surface are fixed in place, and the resulting structures can be reasonably anticipated as a consequence of the hydrophobic attraction between the patches along with steric constraints due to particle shape or other repulsive forces. The preferred number of nearest neighbors, that is, the coordination number, of an amphiphilic particle is determined by the size and the location of the hydrophobic regions on the particle's surface. Despite several elegant strategies for the formation of patchy colloids[10−12] (*e.g.*, by polymer encapsulation of microsphere clusters,[13] masked functionalization using gold vapor deposition,[14] DNA-based interactions,[15−19] or capillary bridges[20,21]), controlling the coordination number of nanoscale particles remains a significant challenge to achieving the programmable self-assembly of nanostructured materials,[22−25] which promise unique mechanical, electronic, and magnetic properties[26] required by emerging applications in energy capture and storage, photonics, and electronics.

Here, we investigate the self-assembly of gold nanoparticles (AuNPs) functionalized with mixed monolayers of hydrophobic and hydrophilic ligands, which are known to rearrange dynamically[27−29] on the particles' surface in response to changes in the local environment (*e.g.*, at liquid interfaces,[27,29,30] within surfactant[28] and lipid[31−33] bilayers). As a consequence, the distribution of hydrophobic ligands on the particles' surface both directs and responds to the organization of the NPs in solution. Under appropriate conditions, these adaptive amphiphiles self-assemble to form linear particle chains with neighboring particles linked together through discrete hydrophobic "bonds" (Figure 1). More generally, by controlling the amount of hydrophobic ligands on the particles' surface, the preferred coordination number of the assembling particles

* Address correspondence to kjmbishop@engr.psu.edu.

Received for review April 2, 2014 and accepted September 17, 2014.

Published online September 17, 2014
10.1021/nn504734v

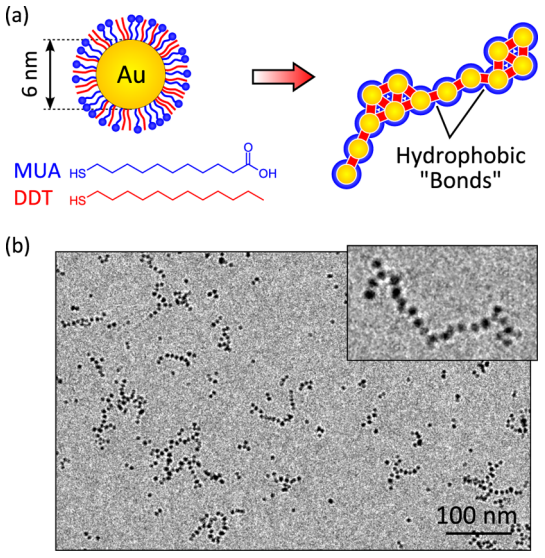

Figure 1. (a) AuNPs functionalized with mixed monolayers of DDT and deprotonated MUA assemble to form chain-like structures in aqueous solutions at high salt concentrations (c_{salt} = 0.2 M) when the surface fraction of DDT ligands is $f \approx 0.25$. (b) Cryo-TEM images of NP chains (c_{Au} = 5 mM, c_{salt} = 0.2 M, $f \approx 0.25$).

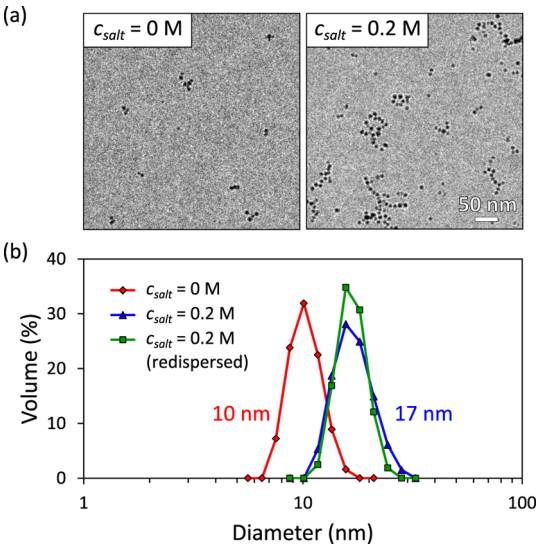

Figure 2. Effect of salt concentration c_{salt}. (a) Cryo-TEM images of 5 mM solutions (on a gold atom basis) of AuMUA/DDT NPs with and without added salt (TMACl) for the DDT coverage, f = 0.25. (b) Cluster size distributions obtained by DLS for the solutions in (a). Precipitation and redispersal of the particles does not influence the final size distribution (compare blue triangles *vs* green squares).

can be varied systematically from ~1 (dimers) to ~2 (linear chains) to ~3 (extended clusters). To explain the experimental observations, we present a simplified model of the particle interactions in which hydrophobic ligands redistribute on the particles' surface to minimize the number of hydrophobe−water contacts. Using these interactions, three-dimensional lattice-based Monte Carlo simulations reproduce the NP structures observed in experiment by cryo-electron microscopy. Together, these results support an assembly mechanism in which the dynamic formation of hydrophobic "sticky" patches guide the formation of NP clusters characterized by a preferred coordination number. The generality of this mechanism is illustrated through additional experiments on amphiphilic cobalt ferrite nanoparticles, which self-assemble in solution to form linear particle clusters under analogous conditions.

RESULTS AND DISCUSSION

Amphiphilic gold nanoparticles (AuNPs; 6.2 ± 0.8 nm diameter) functionalized with mixed monolayers of 11-mercaptoundecanoic acid (MUA) and 1-dodecanethiol (DDT) were prepared by ligand exchange as described previously[28] (see Experimental Section). During surface functionalization, the total number of ligands added (DDT + MUA) was maintained constant, and the molar ratio χ of DDT/MUA varied from 0 to 20. For ligand ratios χ less than ~20, the functionalized particles formed stable dispersions in water (5 mM on a gold atom basis) with the pH adjusted to ~11 by addition of tetramethylammonium hydroxide to fully deprotonate the carboxyl groups.[34] Further increase in the amount of DDT added (χ > 20) caused the particles to aggregate and precipitate from solution.

The ratio of DDT and MUA on the NPs' surface χ_{surf} was determined by titrating the negatively charged AuMUA/DDT NPs with a cationic surfactant (cetyltrimethylammonium tosylate, CTAT), which caused the particles to precipitate sharply at the point of overall charge neutrality.[35] By assuming that (i) the amount of CTAT added is proportional to number of MUA ligands on the NPs' surface and (ii) the ligand ratios χ and χ_{surf} are linearly related as $\chi_{surf} = K\chi$, the constant of proportionality K can be determined by linear regression of the titration data (Supporting Information section A1). Here, K = 0.041 ± 0.005, indicating that MUA adsorbs preferentially to the NP surface. Using this value, we estimated the fraction of DDT on the surface of the NPs as $f = K\chi/(1 + K\chi)$, which ranged from f = 0−0.4 in the experiments. In addition to its simplicity, the electrostatic titration method has been shown to be as accurate as ^{1}H NMR in determining the ratio of ligands on the surface of gold NPs[28,35] (see Supporting Information section A2 for additional NMR characterization).

For the fractional DDT coverage, f = 0.25, amphiphilic NPs formed extended one-dimensional chains as evidenced by cryo-TEM images of NPs in solution (Figure 1b). In many cases, the particle chains were only one NP wide, which suggests the formation of discrete "bonds" between neighboring particles (cf. below). Importantly, particle chains formed only at high salt concentrations (0.2 M tetramethylammonium chloride, TMACl). With no added salt, amphiphilic NPs instead assembled into small clusters (2−4 NPs) with some particles remaining unaggregated as observed by cryo-TEM (Figure 2a).

In addition to cryo-TEM, we confirmed the existence of stable particle aggregates in solution by dynamic light scattering (DLS; Figure 2b), which revealed a unimodal distribution of cluster sizes. The average size of the NP clusters increased with increasing salt concentration from ~10 nm with no added salt to ~17 nm for 0.2 M TMACl (Figure 2b). Importantly, the cluster size distribution remained stable in solution for several months, which suggests that NP clusters are not kinetic precursors to complete precipitation but rather *equilibrium* structures. This hypothesis is further supported by experiments in which NPs were first precipitated by addition of acid to protonate the MUA ligands and then redispersed in a basic salt solution (pH ~ 11, c_{salt} = 0.2 M TMACl). The cluster size distribution of the redispersed NPs was equal (within experimental error) to that of the same particles prior to precipitation under identical conditions (Figure 2b). This observation that cluster size is independent of the initial conditions (dispersed *vs* precipitated) provides additional evidence that NP chains assemble under thermodynamic control.

There are several known mechanisms for achieving chain-like NP aggregates; however, we argue that none are capable of explaining the NP clusters observed here. (1) The present assemblies are equilibrium structures and cannot be explained by diffusion-limited growth mechanisms,[36,37] which lead to structurally similar aggregates[38] under kinetic control. (2) The gold particles used here have no significant magnetic[39,40] or electric[41,42] dipole moments, which can lead to the formation of NP chains through dipolar interactions.[25,43] (3) NP−NP "bonds" are not mediated by chemical cross-linking agents[44] but rather by the hydrophobic ligands on the particles' surface as we demonstrate below. (4) The Debye screening length characterizing the range of electrostatic repulsion between like-charged NPs is only $\kappa^{-1} \approx 0.7$ nm—much smaller than the size of the particles ($\kappa a \approx 7$, where a is the particle radius). Consequently, chain-like structures cannot be explained by a competition of short-ranged hydrophobic attraction and long-ranged electrostatic repulsion, which can lead to the formation of linear particle aggregates[45−47] for larger screening lengths ($\kappa a \sim 0.5$). Here, chain-like assemblies are guided by electrostatic and hydrophobic interactions acting only between neighboring particles in close contact with one another.

To elucidate the mechanism by which NP chains form at high salt concentrations (0.2 M TMACl), we varied the amount of hydrophobic (DDT) ligands on the particles' surface and characterized the resulting structures by cryo-TEM (Figure 3a) and DLS (Figure 3b). In the absence of DDT ligands ($f = 0$), the NPs remained unaggregated in solution with an average hydrodynamic diameter of $d_0 \approx 9$ nm (that of an individual NP). Increasing the DDT fraction to $f = 0.15$, NPs formed

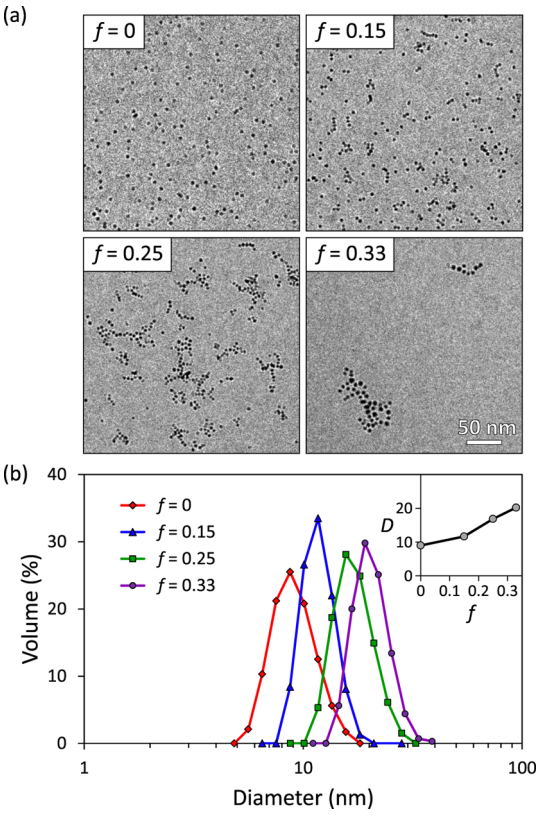

Figure 3. Effect of DDT fraction *f*. (a) Cryo-TEM images of 5 mM solutions of AuMUA/DDT NPs as a function of DDT surface coverage *f* for a common salt concentration c_{salt} = 0.2 M (see Supporting Information section A3 for additional images). The estimated coordination numbers are 0.4 ± 0.7, 1.1 ± 1.1, 1.7 ± 1.1, and 2.9 ± 1.8 for *f* = 0, 0.15, 0.25, and 0.33, respectively (here, ± denotes one standard deviation; see Supporting Information section A4 for details). For *f* = 0.33, the NP clusters often adsorbed to the holey carbon grid, thereby reducing the number of NPs within the field of view. (b) Cluster size distributions for the particles in (a) obtained by DLS; the inset shows the average diameter as a function of DDT fraction *f*.

small linear aggregates of ~2−6 particles with many particles remaining unaggregated in solution. The average hydrodynamic diameter increased to $d \approx$ 12 nm, from which the number of NPs per cluster can be estimated as $(d/d_0)^3 \sim 2$ NPs. We note that the hydrodynamic diameter should be interpreted as a qualitative metric of cluster size as it assumes spherical clusters characterized by an isotropic diffusion coefficient. At $f = 0.25$, longer chains of up to ~10 NPs were observed as well as large branching aggregates; the hydrodynamic diameter was 17 nm (corresponding to ~7 NPs per cluster). Finally, at $f = 0.33$, NPs formed larger, denser aggregates—often with open looplike structures; the hydrodynamic diameter was 20 nm (~11 NPs per cluster). At this relatively high DDT fraction, cryo-TEM imaging became challenging as the NPs adsorbed strongly to the holey carbon TEM grid, thereby reducing the number of NPs visible in the images (see Supporting Information section A3). At higher DDT fractions, the NP clusters were no longer stable in solution.

Taken together, these experiments reveal that both the size of the NP clusters and the extent of chain branching increase with increasing DDT fraction. These observations can be attributed to an increase in the number and/or strength of hydrophobic interactions mediated by DDT ligands on the particles' surface. In particular, analysis of the cyro-TEM images reveals that the average NP coordination number increased monotonically from 0.4, 1.1, 1.7, to 2.9 as the DDT fraction increased from $f = 0$, 0.15, 0.25, to 0.33 (see Supporting Information section A4).

To rationalize these observations, we note that the formation of linear clusters at equilibrium cannot be explained by *isotropic*, short-ranged interactions (electrostatic and/or hydrophobic), which invariably lead to bulk aggregates (see Supporting Information section B5). Therefore, we propose that the attractive hydrophobic forces induced by DDT ligands are instead directed between hydrophobic patches that organize dynamically on the surface of the particles during their assembly. The number of these "sticky" patches depends on the fractional DDT coverage f and directly determines the preferred coordination number of the assembling particles. A similar mechanism has been beautifully demonstrated for micron scale particles[48] and droplets[49] functionalized with surface-mobile DNA linkers, which were shown to concentrate at contacts between particles or droplets presenting DNA with complementary sticky ends.

For the proposed mechanism to be viable, the time scale for ligand reorganization must be considerably faster than the equilibration time of 24 h used in all experiments. The surface diffusion coefficient for thiols on gold surfaces has been estimated previously[50] to be $D_t \sim 10^{-18}$ to 10^{-17} cm^2/s, which corresponds to a characteristic reorganization time of $a^2/D_t \sim 3-30$ h, where a is the NP radius. Additional reports of ligand reorganization on the surface of gold NPs provide an even broader range of time scales. Chechik *et al.* used EPR spectroscopy to probe the lateral diffusion of thiols on AuNPs and found that ligand diffusion at room temperature requires several days.[51] On the other hand, the experiments of Bjørnholm *et al.* on amphiphilic NPs—similar to those used here—suggest that ligand rearrangement can proceed within minutes in the presence of strong driving forces (*e.g.*, that which motivates the migration of a polar molecule from an organic phase to water).[29] In our experiments, NP structures were equilibrated for at least 24 h, and we find no differences in the structures that form when we equilibrate for longer times (up to months). This suggests that ligand reorganization (assuming it does indeed occur) proceeds on time scales shorter than 24 h.

To demonstrate the importance of ligand reorganization on the formation of NP aggregates, we prepared amphiphilic NPs using short assembly times—shorter than that of ligand reorganization—and characterized the resulting structures by cryo-TEM. Initially, amphiphilic NPs (DDT fraction, $f = 0.25$) were dispersed in water with no added salt (see Figure 2a, left). Addition of 0.2 M TMACl effectively screened the electrostatic repulsions between the negatively charged particles and allowed for their aggregation into chain-like assemblies (see Figure 2a, right). When, however, this aggregation process was arrested after only ~1 min, we found no such structures under cryo-TEM (see Supporting Information section A5). Instead, the NPs remained largely unaggregated despite frequent collisions at rate of $\sim 10^3$ s^{-1} as estimated from the Smoluchowski equation. Briefly, the rate of diffusion-limited encounters between spheres of radius a and concentration C is on the order of $16\pi aDC$, where $D \approx k_BT/3\pi\eta d$ is the Stokes—Einstein diffusivity of the particles in a liquid with viscosity η and temperature T. Thus, while NPs encounter one another frequently in solution, they rarely stick effectively. This result is consistent with the proposed assembly mechanism in which the rate of aggregation is limited by that of ligand reorganization on the NPs' surface.

The proposed assembly mechanism is further supported by 3D lattice Monte Carlo simulations incorporating a simplified model of the NP interactions that combines (i) short-ranged hydrophobic attraction, (ii) dynamic rearrangement of the DDT ligands on the NPs' surface, and (iii) short-ranged electrostatic repulsion. As we show below, this model reproduces and explains the formation of linear NP aggregates as well as the observed dependencies on the DDT fraction.

In the model, each particle is covered by N_L total ligands of which H are hydrophobic (such that $f = H/N_L$). Each contact between a hydrophobic ligand and the aqueous solvent is assumed to contribute a constant amount ε_{hp} to the total energy of the system (here, $\varepsilon_{hp} \sim 1\ k_BT$ assuming a characteristic oil—water surface energy of 20 mJ/m^2 and a ligand area[52] of 0.2 nm^2). When two NPs make contact, a patch is formed to which a hydrophobic ligand can move to reduce the energy of the system by an amount ε_{hp}. To keep track of these interactions, let H_{ij} denote the number of hydrophobic ligands on particle i located within the "patch" formed with particle j. The numbers of "bonding" ligands (H_{ij} with $i \neq j$) and "nonbonding" ligands (H_{ii}) obey the relations

$$H_{ij} \geq 0 \quad \text{and} \quad \sum_{j=1}^{N_p} H_{ij} = H \tag{1}$$

where N_p is the total number of particles. These relations imply that (i) the number of ligands contributing to each bond is nonnegative and (ii) the total number of ligands on each particle is H. Furthermore, we assume that only neighboring particles can form

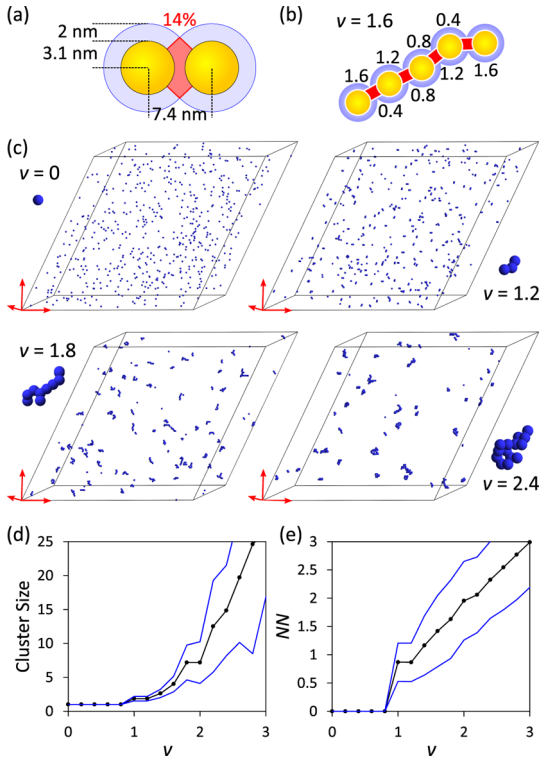

Figure 4. (a) Idealized geometry of a NP−NP contact. The ligand length of ∼2 nm sets the range of hydrophobic interactions; the particle separation was chosen to accommodate the volume of the ligands within the contact region. (b) Minimum energy ligand distribution for a linear cluster with coordination parameter v = 1.6; all hydrophobic ligands are accommodated within contact regions. (c−e) Results of MC simulations with particle density $\rho = 2 \times 10^{-4}$, hydrophobic bond strength β = 100, and electrostatic repulsion $\alpha = 90$ for four different values of the coordination parameter v corresponding to the conditions of experiments shown in Figure 3. (c) Equilibrium particle configurations. Chain-like assemblies similar to those from Figure 1b were observed for v = 1.8. (d) Average cluster size (black markers) as a function of the parameter v; blue curves denote one standard deviation above and below the mean. (e) Average number of nearest neighbors NN (black markers) as a function of v; blue curves denote one standard deviation above and below the mean.

hydrophobic bonds such that $H_{ij} = 0$ when particles i and j are not nearest neighbors. Finally, to account for the geometric constraints on the maximum number of hydrophobic ligands located between two spherical particles, we specify an upper bound on the number of ligands that can contribute to a single bond.

$$H_{ij} + H_{ji} \leq 2H_{\max} \quad \text{for} \quad i \neq j \tag{2}$$

Physically, $H_{\max}$ depends on the length of the hydrophobic ligands relative to the size of the particles; for the idealized NP−NP contact illustrated in Figure 4a, we estimate that $H_{\max} \approx 0.136H$. Additionally, when three or four NPs come into mutual contact, their contact regions overlap and it is necessary to reduce the effective size of the contact to $H^{(3)}_{\max} \approx 0.122H$ and $H^{(4)}_{\max} \approx 0.110H$, respectively (see Supporting Information section B1 for details).

With these preliminaries, the total energy E_{hp} due to contacts between hydrophobic ligands and water is expressed as

$$E_{hp} = \varepsilon_{hp} \sum_{i=1}^{N_P} H_{ii} \tag{3}$$

To account for the dynamics of hydrophobic DDT ligands on the particles' surface, we make an important simplifying assumption—namely, that the distribution of hydrophobic ligands equilibrates to the minimum energy configuration. Mathematically, we identify the ligand distribution H_{ij} that minimizes the hydrophobic energy (3) subject to the constraints (1) and (2). The solution to this constrained optimization problem can be obtained rapidly and uniquely using standard methods of linear programming. Figure 4b shows the minimum energy ligand distribution for a simple linear cluster of five NPs.

Interestingly, we note that the resulting hydrophobic energy E_{hp} cannot be obtained by summing over local, pairwise interactions. The distribution of hydrophobic ligands on the particles' surface is determined by the complete topology of the particle aggregates. As a consequence, the addition of one NP to one part of a cluster results in a cascading rearrangement of the hydrophobic ligands to achieve the new minimum energy configuration. Such "global" interactions are necessary to explain the formation of the one-dimensional chains observed in experiment.

At high salt conditions, the Debye screening length is small relative to the particle size, and repulsive electrostatic interactions are limited to those between nearest neighbors. In particular, we assume that each of the M nearest neighbor interactions contributes a fixed amount ε_{es} to the total electrostatic energy, $E_{es} = \varepsilon_{es}M$. The magnitude of the electrostatic interaction ε_{es} between two charged NPs at contact was estimated using the nonlinear Poisson−Boltzmann equation to be $\varepsilon_{es} \approx 120\ k_BT$ for the experimental conditions (see Supporting Information section B2).

Using the interactions above, we performed Monte Carlo (MC) simulations (NVT ensemble) on a collection of N_p = 549 particles interacting on a cubic close-packed (ccp) lattice. For a given particle configuration, the total energy of the system E was approximated as the sum of hydrophobic and electrostatic contributions, $E = E_{hp} + E_{es}$. The equilibrium distribution of particle configurations was sampled using the standard Metropolis−Hastings algorithm[53] with single particle "exchange" moves and periodic boundaries (see Experimental Section for details). These MC moves allowed for the direct exchange of particles between different clusters and were necessary to accelerate the equilibration of the system at the dilute NP concentrations used in experiment (see Supporting Information section B3).

The model is characterized by four dimensionless parameters that uniquely specify the behavior of the system: (1) the particle density, $\rho = N_p/N_s$, where N_s is the number of lattice sites; (2) the number of hydrophobic ligands per particle, $v = H/H_{max}$, where H_{max} is the maximum number of ligands per bond; (3) the characteristic strength of a hydrophobic bond, $\beta = 2\varepsilon_{np}H_{max}/k_BT$, where k_BT is the thermal energy; and (4) the strength of the electrostatic repulsion, $\alpha = \varepsilon_{es}/k_BT$. In the simulations, the particle density ρ was chosen to correspond to the experimental value of $\rho = 2 \times 10^{-4}$. The hydrophobic bond strength is estimated to be on the order of $\beta \sim 100$, which is similar in magnitude to the electrostatic repulsion $\alpha \sim 100$. While both attractive and repulsive forces are strong (relative to thermal motion), the former must be considerably stronger than the latter to induce NP aggregation; that is, $\beta - \alpha \gg 1$. In the simulations, we chose $\beta = 100$ and $\alpha = 90$ to capture the essential features of the experimental system.

Figure 4c shows simulation snapshots of the equilibrium NP configuration for different values of the coordination parameter $v = 0$, 1.2, 1.8, and 2.4 corresponding to DDT fractions f similar to those used in experiment (cf. Figure 3). The model captures the experimentally observed progression from free NPs ($v = 0$) to short linear chains ($v = 1.2$) to longer branched chains ($v = 1.8$) to denser aggregates ($v = 2.4$). The average size of these equilibrium clusters increased exponentially with increasing number of hydrophobic ligands on the particles' surface (Figure 4d); in particular, the cluster size increased from 1 to 2 to 7 to 15 NPs for the conditions in Figure 4c, in good agreement with estimates from DLS measurements. In addition to reproducing the experimental observations, the model can offer additional insights into the structure of the NP clusters. In particular, we find that the average number of nearest neighbors NN increases linearly with the number of hydrophobic ligands on the particles' surface; that is, NN $\approx v$ (Figure 4e). This result suggests that the assembling particles have a preferred coordination number, as determined by the competition between hydrophobic attraction and electrostatic repulsion.

To understand the formation of chain-like aggregates in the model, consider that all the hydrophobic groups can be shielded from the solvent provided each particle has *ca.* v or more nearest neighbors. The formation of additional neighbors—beyond that needed to shield the hydrophobic ligands—is strongly penalized by the repulsive electrostatic interactions. Thus, for $v = 1.8$, NPs form aggregates with 1.6 ± 0.7 nearest neighbors (where $\pm$ refers to one standard deviation). Under dilute conditions, one might expect such particles to form trimers rather than extended chains as (i) both structures have *ca.* two "bonds" per NP and (ii) small clusters are favored for entropic reasons. The formation of chain-like structures is a direct consequence of ligand redistribution, which can enable a linear cluster of N particles to shield all of its hydrophobic ligands within $N - 1$ bonds (provided $N \geq 2/(2 - v)$; see Figure 4b). By contrast, a trimer of $N = 3$ particles requires $N = 3$ bonds to shield its hydrophobic ligands, resulting in an energy difference of $\alpha(N - 1)/N$ per particle ($\sim 90\, k_BT$ for $v = 1.8$). As a result, extended chain-like clusters are favored over smaller trimers. At higher DDT fractions ($v > 2$), the formation of more open, extended structures is also driven by geometric factors: the formation of large hydrophobic patches between neighboring particles favors NP configurations with few three-particle (triangular) and four-particle (tetrahedral) contacts. This effect leads to the formation of open looplike structures observed in experiment ($f = 0.33$) and in simulations ($v = 2.4$).

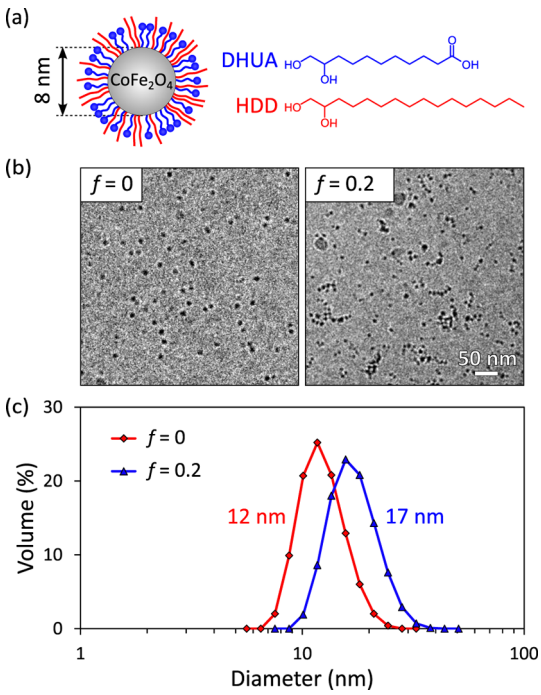

Figure 5. (a) $CoFe_2O_4$ NPs functionalized with mixed monolayers of HDD and deprotonated DHUA assemble to form chain-like structures in aqueous solutions at high salt concentrations (c_{salt} = 0.2 M) when the surface fraction of HDD ligands is $f \approx 0.2$. (b) Cryo-TEM images and (c) DLS size distributions of NP chains ($c_{CoFe_2O_4}$ = 6.66 mg/mL, c_{salt} = 0.2 M, and $f \approx 0$ and 0.2).

Finally, to demonstrate the generality of this mechanism, we applied a similar procedure to assemble particle chains using cobalt ferrite nanoparticles ($CoFe_2O_4$ NPs; 8.2 $\pm$ 1.4 nm in diameter) functionalized with chemically similar hydrophobic (1,2-hexadecanediol, HDD) and hydrophilic (10,11-dihydroxyundecanoic acid, DHUA; fully deprotonated at pH $\approx$ 11) ligands (Figure 5a). As with the AuNP system, we investigated the structures formed by amphiphilic $CoFe_2O_4$ NPs using cryo-TEM and DLS (Figure 5b,c). At high salt conditions (0.2 M TMACl) and HDD coverage $f = 0.2$, amphiphilic $CoFe_2O_4$ NPs assemble into short linear chains similar to those of

the gold NPs with an average hydrodynamic diameter of 17 nm (~3 particles). By contrast, little or no particle clustering was observed in the absence of hydrophobic ligands ($f = 0$) as evidenced by cryo-TEM; the average hydrodynamic diameter was 12 nm (that of single NPs). These observations suggest that chain formation was mediated by hydrophobic interactions between HDD ligands rather by dipolar interactions between the NP cores.

The strength of magnetic dipole−dipole interactions between proximal NPs is not sufficient to induce chain-like ordering. The attractive dipole−dipole energy of two NPs in contact is $U_{dd} = m^2/2\pi\mu_0 d^3 \approx 0.5\ k_B T$, where $m = \mu_0 V M_S$ is the particle's magnetic moment, μ_0 is the vacuum permeability, V is the particle volume, $M_S = 2.7 \times 10^5$ A/m is the saturation magnetization,[54] and $d = 8.2$ nm is the particle diameter. The formation of chain-like assemblies *via* magnetic dipole−dipole interactions requires significantly larger particles, for which the strength of the magnetic interactions is several times the thermal energy.[40,55] Instead, we attribute the formation of chain-like structures to hydrophobic interactions between the HDD ligands in direct analogy to the DDT ligands in the AuNP system.

CONCLUSIONS

Nanoparticle amphiphiles functionalized with both hydrophobic (DDT) and hydrophilic (MUA) ligands self-assemble to form equilibrium clusters characterized by a preferred coordination number, which depends on the number of hydrophobic ligands on the particles' surface. In particular, NPs at high salt conditions (0.2 M TMACl) and DDT coverage ($f = 0.25$) assemble to form extended chain-like structures through attractive hydrophobic interactions between DDT ligands bound to proximal NPs. To explain the formation of these linear clusters, we propose an assembly mechanism whereby hydrophobic patches organize between neighboring particles to minimize the number of energetically unfavorable DDT−water contacts. This mechanism is supported by Monte Carlo simulations incorporating adaptive hydrophobic interactions that reproduce the structures and trends observed in the experiment. The extension of these results to different NP materials and ligand chemistries (namely, $CoFe_2O_4$/DHUA/HDD NPs) suggests that this mechanism is general to other materials, provided that the ligands are sufficiently mobile on the time scales of interest. By contrast to amphiphilic particles with "fixed" surface chemistries, adaptive amphiphiles with mobile ligands may provide an easy route for controlling particle coordination number within NP assemblies. Beyond linear chains, such particles may be capable of forming well-defined "equilibrium gels" in which particles interact with a prescribed number of nearest neighbors to yield space-filling networks. At present, this strategy can specify only the preferred number of nearest neighbor "bonds" but not their orientations. It may, however, be possible to extend the present approach to create *directional* bonds through a combination of adaptive hydrophobic attraction and long-range electrostatic repulsion, for example, to guide the formation of non-close-packed nanoparticle assemblies.[13,56,57]

EXPERIMENTAL SECTION

Materials. Tetra-*n*-butylammonium borohydride (TBAB, 98%), 1-dodecanethiol (DDT, 98%), and tetramethylammonium choloride (TMACl, 97%) were obtained from Alfa Aesar. 11-Mercaptoundecanoic acid (MUA, 95%), dodecylamine (DDA, 98%), hydrazine (anhydrous, 98%), tetramethylammonium hydroxide (TMAOH, 25 wt % solution in water), cetyltrimethylammonium tosylate (CTAT), iodine, deuterated dichloromethane, gold chloride trihydrate crystal ($HAuCl_4 \cdot 3H_2O$), cobalt(II) acetylacetonate ($Co(acac)_2$, 97%), 1,2-tetradecanediol (TDD, 90%), benzyl ether (98%), oleic acid (OA, 90%), oleylamine (OAm, >70%), 10-undecanoic acid (98%), formic acid (98%), and diethyl ether (>99.9%) were obtained from Sigma-Aldrich. Iron(III) acetylacetonate ($Fe(acac)_3$, 97%) was obtained from Strem Chemicals. Hydrogen peroxide (30% w/w) and sodium hydroxide were obtained from BDH chemicals. Didodecyldimethylammonium bromide (DDAB) and 1,2-hexadecanediol (HDD, >98%) were obtained from TCI. Dichloromethane, toluene, methanol, ethanol, chloroform, hydrochloric acid, and acetone were obtained from EMD chemicals. All chemicals were used without further purification.

Nanoparticle Synthesis and Surface Funtionalization. Gold nanoparticles (AuNPs; 6.2 ± 0.8 nm diameter) were synthesized according to a modified literature procedure[57,58] using $HAuCl_4 \cdot 3H_2O$ instead of $AuCl_3$. Initially, the particles were stabilized by weakly bound DDA ligands and dispersed in toluene. The surface of the AuDDA particles was then functionalized with mixed monolayers of MUA and DDT *via* ligand exchange. Briefly, 0−40 μmol of DDT dissolved in toluene (0−2 mL of 20 mM solution) was added to 10 μmol AuDDA (0.5 mL of 20 mM solution on a gold atom basis) and stirred gently for 2 min. Subsequent addition of 0−40 μmol of MUA dissolved in dichloromethane (0−2 mL of 20 mM solution), followed by 12 h of stirring at room temperature, caused the particles to precipitate from solution. After the supernatant was decanted, the functionalized AuMUA/DDT particles were washed with toluene, dichloromethane, and acetone to remove excess ligands, dried with nitrogen, and dissolved in 2 mL of deionized water with pH adjusted to >11 by addition of TMAOH. Finally, the samples were sonicated for 10 min and allowed to equilibrate for at least 24 h unless otherwise stated.

Cobalt ferrite nanoparticles (8.2 ± 1.4 nm diameter) were synthesized according to a modified literature procedure using TDD instead of HDD.[59] As with the AuNPs, the particles were initially stabilized by oleic acid and oleylamine ligands in toluene and then functionalized with mixed monolayers of HDD and DHUA *via* ligand exchange [DHUA was synthesized according to a literature procedure;[60] ^{1}H NMR (DMSO-d_6): δ (ppm) = 1.17−1.30 (m, 10H, $(CH_2)_5CH_2CH_2COOH$), 1.38−1.39 (m, 2H, CH_2CHOH), 1.4−1.5 (m, 2H, CH_2CH_2COOH), 2.16−2.2 (t, 2H, CH_2COOH), 3.21−3.24 (m, 2H, CH_2OH), 3.35 (m, 1H, *CH*OH), 4.2−4.4 (br s, 2H, O*H*), 11.99 (br s, 1H, COO*H*)]. Briefly, 0−109 μmol of HDD dissolved in chloroform (0−1.6 mL of 70 mM solution) was added to 6 mg of $CoFe_2O_4$ stabilized by OA and OAm in toluene and agitated gently for 2 min. Then, 0−110 μmol of DHUA dissolved in ethanol (0−11 mL of 10 mM solution) was added to the solution, followed by stirring

for 12 h at room temperature. Addition of excess of ethanol caused the particles to precipitate from the solution, and after the supernatant was decanted, DHUA/HDD-functionalized $CoFe_2O_4$ NPs were washed with ethanol and acetone to remove excess ligands, dried with nitrogen, and dissolved in deionized water with pH adjusted to >11 by addition of TMAOH. Finally, after the samples were centrifuged to remove aggregated NPs, the samples were sonicated for 10 min and allowed to equilibrate for at least 24 h.

Nanoparticle Characterization. Cryo-TEM measurements were taken on FEI Tecnai G2 Spirit Bio Twin operating at 120 kV accelerating voltage and attached to bottom-mount Eagle 4 k HS camera for image collection. To help preserve the NP aggregates during sample preparation, vitrified specimens were prepared in the semiautomated Vitrobot, a closed chamber at 20 °C and 100% relative humidity. Dynamic light scattering measurements were performed on a Malvern Zetasizer Nano ZS90 equipped with a 4 mW HeNe gas laser operating at a wavelength of 632.8 nm and a scattering angle of 90°. All samples were measured at room temperature.

Monte Carlo Simulations. All simulations were performed on a ccp lattice (140 × 140 × 140) containing $N_p = 529$ particles, which were initially distributed at random. Before the equilibrium configuration was sampled, the system was first equilibrated over the course of 10^3 N_p attempted MC moves. To accelerate the equilibration of NP clusters under dilute conditions, we developed an efficient MC move that allows for the direct exchange of particles between clusters while maintaining the detailed balance condition[53] required for sampling the equilibrium distribution (see Supporting Information section B3).

Conflict of Interest: The authors declare no competing financial interest.

Acknowledgment. This work was supported by the Nonequilibrium Energy Research Center (NERC), an Energy Frontier Research Center funded by the U.S. Department of Energy under Award Number DE-SC0000989.

Supporting Information Available: Electrostatic titration data; ligand composition by ^{1}H NMR; additional cryo-TEM images; cryo-TEM image analysis; estimation of electrostatic interactions; additional simulation data on the role of anisotropic interactions. This material is available free of charge *via* the Internet at http://pubs.acs.org.

REFERENCES AND NOTES

1. Hong, L.; Cacciuto, A.; Luijten, E.; Granick, S. Clusters of Amphiphilic Colloidal Spheres. *Langmuir* **2008**, *24*, 621–625.
2. Chen, Q.; Whitmer, J. K.; Jiang, S.; Bae, S. C.; Luijten, E.; Granick, S. Supracolloidal Reaction Kinetics of Janus Spheres. *Science* **2011**, *331*, 199–202.
3. Larson-Smith, K.; Pozzo, D. C. Scalable Synthesis of Self-Assembling Nanoparticle Clusters Based on Controlled Steric Interactions. *Soft Matter* **2011**, *7*, 5339–5347.
4. He, J.; Huang, X. L.; Li, Y. C.; Liu, Y. J.; Babu, T.; Aronova, M. A.; Wang, S. J.; Lu, Z. Y.; Chen, X. Y.; Nie, Z. H. Self-Assembly of Amphiphilic Plasmonic Micelle-like Nanoparticles in Selective Solvents. *J. Am. Chem. Soc.* **2013**, *135*, 7974–7984.
5. He, J.; Liu, Y. J.; Babu, T.; Wei, Z. J.; Nie, Z. H. Self-Assembly of Inorganic Nanoparticle Vesicles and Tubules Driven by Tethered Linear Block Copolymers. *J. Am. Chem. Soc.* **2012**, *134*, 11342–11345.
6. He, J.; Wei, Z. J.; Wang, L.; Tomova, Z.; Babu, T.; Wang, C. Y.; Han, X. J.; Fourkas, J. T.; Nie, Z. H. Hydrodynamically Driven Self-Assembly of Giant Vesicles of Metal Nanoparticles for Remote-Controlled Release. *Angew. Chem., Int. Ed.* **2013**, *52*, 2463–2468.
7. Chen, Q.; Bae, S. C.; Granick, S. Directed Self-Assembly of a Colloidal Kagome Lattice. *Nature* **2011**, *469*, 381–384.
8. Cademartiri, L.; Bishop, K. J. M.; Snyder, P. W.; Ozin, G. A. Using Shape for Self-Assembly. *Philos. Trans. R. Soc., A* **2012**, *370*, 2824–2847.
9. Sacanna, S.; Pine, D. J. Shape-Anisotropic Colloids: Building Blocks for Complex Assemblies. *Curr. Opin. Colloid Interface Sci.* **2011**, *16*, 96–105.
10. Zhang, Z. L.; Glotzer, S. C. Self-Assembly of Patchy Particles. *Nano Lett.* **2004**, *4*, 1407–1413.
11. Pawar, A. B.; Kretzschmar, I. Fabrication, Assembly, and Application of Patchy Particles. *Macromol. Rapid Commun.* **2010**, *31*, 150–168.
12. Glotzer, S. C.; Solomon, M. J. Anisotropy of Building Blocks and Their Assembly into Complex Structures. *Nat. Mater.* **2007**, *6*, 557–562.
13. Wang, Y. F.; Wang, Y.; Breed, D. R.; Manoharan, V. N.; Feng, L.; Hollingsworth, A. D.; Weck, M.; Pine, D. J. Colloids with Valence and Specific Directional Bonding. *Nature* **2012**, *491*, 51–56.
14. Pawar, A. B.; Kretzschmar, I. Patchy Particles by Glancing Angle Deposition. *Langmuir* **2008**, *24*, 355–358.
15. Feng, L.; Dreyfus, R.; Sha, R. J.; Seeman, N. C.; Chaikin, P. M. DNA Patchy Particles. *Adv. Mater.* **2013**, *25*, 2779–2783.
16. Ke, Y. G.; Ong, L. L.; Shih, W. M.; Yin, P. Three-Dimensional Structures Self-Assembled from DNA Bricks. *Science* **2012**, *338*, 1177–1183.
17. Wei, B.; Dai, M. J.; Yin, P. Complex Shapes Self-Assembled from Single-Stranded DNA Tiles. *Nature* **2012**, *485*, 623–626.
18. Iinuma, R.; Ke, Y. G.; Jungmann, R.; Schlichthaerle, T.; Woehrstein, J. B.; Yin, P. Polyhedra Self-Assembled from DNA Tripods and Characterized with 3D DNA-Paint. *Science* **2014**, *344*, 65–69.
19. Sadowski, J. P.; Calvert, C. R.; Zhang, D. Y.; Pierce, N. A.; Yin, P. Developmental Self-Assembly of a DNA Tetrahedron. *ACS Nano* **2014**, *8*, 3251–3259.
20. Kamalasanan, K.; Jhunjhunwala, S.; Wu, J. M.; Swanson, A.; Gao, D.; Little, S. R. Patchy, Anisotropic Microspheres with Soft Protein Islets. *Angew. Chem., Int. Ed.* **2011**, *50*, 8706–8708.
21. Hijnen, N.; Clegg, P. S. Colloidal Aggregation in Mixtures of Partially Miscible Liquids by Shear-Induced Capillary Bridges. *Langmuir* **2014**, *30*, 5763–5770.
22. Li, F.; Josephson, D. P.; Stein, A. Colloidal Assembly: The Road from Particles to Colloidal Molecules and Crystals. *Angew. Chem., Int. Ed.* **2011**, *50*, 360–388.
23. Ozin, G. A.; Hou, K.; Lotsch, B. V.; Cademartiri, L.; Puzzo, D. P.; Scotognella, F.; Ghadimi, A.; Thomson, J. Nanofabrication by Self-Assembly. *Mater. Today* **2009**, *12*, 12–23.
24. Velev, O. D.; Gupta, S. Materials Fabricated by Micro- and Nanoparticle Assembly: The Challenging Path from Science to Engineering. *Adv. Mater.* **2009**, *21*, 1897–1905.
25. Bishop, K. J. M.; Wilmer, C. E.; Soh, S.; Grzybowski, B. A. Nanoscale Forces and Their Uses in Self-Assembly. *Small* **2009**, *5*, 1600–1630.
26. Cademartiri, L.; Ozin, G. A. *Concepts of Nanochemistry*; Wiley-VCH: Weinheim, Germany, 2009.
27. Andala, D. M.; Shin, S. H. R.; Lee, H. Y.; Bishop, K. J. M. Templated Synthesis of Amphiphilic Nanoparticles at the Liquid−Liquid Interface. *ACS Nano* **2012**, *6*, 1044–1050.
28. Lee, H. Y.; Shin, S. H. R.; Abezgauz, L. L.; Lewis, S. A.; Chirsan, A. M.; Danino, D. D.; Bishop, K. J. M. Integration of Gold Nanoparticles into Bilayer Structures *via* Adaptive Surface Chemistry. *J. Am. Chem. Soc.* **2013**, *135*, 5950–5953.
29. Norgaard, K.; Weygand, M. J.; Kjaer, K.; Brust, M.; Bjørnholm, T. Adaptive Chemistry of Bifunctional Gold Nanoparticles at the Air/Water Interface. A Synchrotron X-ray Study of Giant Amphiphiles. *Faraday Discuss.* **2004**, *125*, 221–233.
30. Sashuk, V.; Winkler, K.; Zywocinski, A.; Wojciechowski, T.; Gorecka, E.; Fialkowski, M. Nanoparticles in a Capillary Trap: Dynamic Self-Assembly at Fluid Interfaces. *ACS Nano* **2013**, *7*, 8833–8839.
31. Carney, R. P.; Astier, Y.; Carney, T. M.; Voitchovsky, K.; Silva, P. H. J.; Stellacci, F. Electrical Method To Quantify Nanoparticle Interaction with Lipid Bilayers. *ACS Nano* **2013**, *7*, 932–942.
32. Lehn, R. C. V.; Atukorale, P. U.; Carney, R. P.; Yang, Y.-S.; Stellacci, F.; Irvine, D. J.; Alexander-Katz, A. Effect of Particle Diameter and Surface Composition on the Spontaneous

Fusion of Monolayer-Protected Gold Nanoparticles with Lipid Bilayers. *Nano Lett.* **2013**, *13*, 4060–4067.
33. Lehn, R. C. V.; Ricci, M.; Silva, P. H. J.; Andreozzi, P.; Reguera, J.; Voïtchovsky, K.; Stellacci, F.; Alexander-Katz, A. Lipid Tail Protrusions Mediate the Insertion of Nanoparticles into Model Cell Membranes. *Nat. Commun.* **2014**, *5*, 4482.
34. Wang, D. W.; Nap, R. J.; Lagzi, I.; Kowalczyk, B.; Han, S. B.; Grzybowski, B. A.; Szleifer, I. How and Why Nanoparticle's Curvature Regulates the Apparent pK_a of the Coating Ligands. *J. Am. Chem. Soc.* **2011**, *133*, 2192–2197.
35. Kalsin, A. M.; Kowalczyk, B.; Wesson, P.; Paszewski, M.; Grzybowski, B. A. Studying the Thermodynamics of Surface Reactions on Nanoparticles by Electrostatic Titrations. *J. Am. Chem. Soc.* **2007**, *129*, 6664–6665.
36. Turkevich, L. A.; Scher, H. Occupancy-Probability Scaling in Diffusion-Limited Aggregation. *Phys. Rev. Lett.* **1985**, *55*, 1026–1029.
37. Lin, M. Y.; Lindsay, H. M.; Weitz, D. A.; Klein, R.; Ball, R. C.; Meakin, P. Universal Diffusion-Limited Aggregation. *J. Phys.: Condens. Matter* **1990**, *2*, 3093–3113.
38. Enustun, B. V.; Turkevich, J. Coagulation of Colloidal Gold. *J. Am. Chem. Soc.* **1963**, *85*, 3317–3328.
39. Wang, H.; Chen, Q. W.; Sun, Y. B.; Wang, M. S.; Sun, L. X.; Yan, W. S. Synthesis of Necklace-like Magnetic Nanorings. *Langmuir* **2010**, *26*, 5957–5962.
40. Klokkenburg, M.; Vonk, C.; Claesson, E. M.; Meeldijk, J. D.; Erne, B. H.; Philipse, A. P. Direct Imaging of Zero-Field Dipolar Structures in Colloidal Dispersions of Synthetic Magnetite. *J. Am. Chem. Soc.* **2004**, *126*, 16706–16707.
41. Tang, Z. Y.; Ozturk, B.; Wang, Y.; Kotov, N. A. Simple Preparation Strategy and One-Dimensional Energy Transfer in Cdte Nanoparticle Chains. *J. Phys. Chem. B* **2004**, *108*, 6927–6931.
42. Tang, Z. Y.; Kotov, N. A.; Giersig, M. Spontaneous Organization of Single CdTe Nanoparticles into Luminescent Nanowires. *Science* **2002**, *297*, 237–240.
43. Tang, Z. Y.; Kotov, N. A. One-Dimensional Assemblies of Nanoparticles: Preparation, Properties, and Promise. *Adv. Mater.* **2005**, *17*, 951–962.
44. DeVries, G. A.; Brunnbauer, M.; Hu, Y.; Jackson, A. M.; Long, B.; Neltner, B. T.; Uzun, O.; Wunsch, B. H.; Stellacci, F. Divalent Metal Nanoparticles. *Science* **2007**, *315*, 358–361.
45. Campbell, A. I.; Anderson, V. J.; van Duijneveldt, J. S.; Bartlett, P. Dynamical Arrest in Attractive Colloids: The Effect of Long-Range Repulsion. *Phys. Rev. Lett.* **2005**, *94*, 208301.
46. Toledano, J. C. F.; Sciortino, F.; Zaccarelli, E. Colloidal Systems with Competing Interactions: From an Arrested Repulsive Cluster Phase to a Gel. *Soft Matter* **2009**, *5*, 2390–2398.
47. Zhang, T. H.; Klok, J.; Tromp, R. H.; Groenewold, J.; Kegel, W. K. Non-equilibrium Cluster States in Colloids with Competing Interactions. *Soft Matter* **2012**, *8*, 667–672.
48. van der Meulen, S. A. J.; Leunissen, M. E. Solid Colloids with Surface-Mobile DNA Linkers. *J. Am. Chem. Soc.* **2013**, *135*, 15129–15134.
49. Feng, L.; Pontani, L. L.; Dreyfus, R.; Chaikin, P.; Brujic, J. Specificity, Flexibility and Valence of DNA Bonds Guide Emulsion Architecture. *Soft Matter* **2013**, *9*, 9816–9823.
50. Imabayashi, S.; Hobara, D.; Kakiuchi, T. Voltammetric Detection of the Surface Diffusion of Adsorbed Thiolate Molecules in Artificially Phase-Separated Binary Self-Assembled Monolayers on a Au(111) Surface. *Langmuir* **2001**, *17*, 2560–2563.
51. Ionita, P.; Volkov, A.; Jeschke, G.; Chechik, V. Lateral Diffusion of Thiol Ligands on the Surface of Au Nanoparticles: An Electron Paramagnetic Resonance Study. *Anal. Chem.* **2008**, *80*, 95–106.
52. Leff, D. V.; Ohara, P. C.; Heath, J. R.; Gelbart, W. M. Thermodynamic Control of Gold Nanocrystal Size: Experiment and Theory. *J. Phys. Chem.* **1995**, *99*, 7036–7041.
53. Frenkel, D.; Smit, B. *Understanding Molecular Simulation*, 2nd ed.; Academic Press: New York, 2001.
54. Maaz, K.; Mumtaz, A.; Hasanain, S. K.; Ceylan, A. Synthesis and Magnetic Properties of Cobalt Ferrite ($CoFe_2O_4$) Nanoparticles Prepared by Wet Chemical Route. *J. Magn. Magn. Mater.* **2007**, *308*, 289–295.
55. Nakata, K.; Hu, Y.; Uzun, O.; Bakr, O.; Stellacci, F. Chains of Superparamagnetic Nanoplarticles. *Adv. Mater.* **2008**, *20*, 4294–4299.
56. Bishop, K. J. M.; Chevalier, N. R.; Grzybowski, B. A. When and Why Like-Sized, Oppositely Charged Particles Assemble into Diamond-like Crystals. *J. Phys. Chem. Lett.* **2013**, *4*, 1507–1511.
57. Kalsin, A. M.; Fialkowski, M.; Paszewski, M.; Smoukov, S. K.; Bishop, K. J. M.; Grzybowski, B. A. Electrostatic Self-Assembly of Binary Nanoparticle Crystals with a Diamond-like Lattice. *Science* **2006**, *312*, 420–424.
58. Jana, N. R.; Peng, X. G. Single-Phase and Gram-Scale Routes toward Nearly Monodisperse Au and Other Noble Metal Nanocrystals. *J. Am. Chem. Soc.* **2003**, *125*, 14280–14281.
59. Sun, S. H.; Zeng, H.; Robinson, D. B.; Raoux, S.; Rice, P. M.; Wang, S. X.; Li, G. X.; Monodisperse, M. Fe_2O_4 (M = Fe, Co, Mn) Nanoparticles. *J. Am. Chem. Soc.* **2004**, *126*, 273–279.
60. Swern, D.; Billen, G. N.; Findley, T. W.; Scanlan, J. T. Hydroxylation of Monosaturated Fatty Materials with Hydrogen Peroxide. *J. Am. Chem. Soc.* **1945**, *67*, 1786–1789.